Available online at www.sciencedirect.com
ScienceDirect
Comput. Methods Appl. Mech. Engrg. 278 (2014) 145–159
Computer methods in applied mechanics and engineering
www.elsevier.com/locate/cma

Boundary effects in a phase-field approach to topology optimization

Mathias Wallin*, Matti Ristinmaa

Division of Solid Mechanics, Lund University, Box 118, SE-22100 Lund, Sweden

Received 25 September 2013; received in revised form 17 March 2014; accepted 8 May 2014
Available online 28 May 2014

Highlights

- A boundary term is included in the phase-field approach which enables control of outer boundaries.
- The box constraints enforcing the upper and lower limits are included via an obstacle potential.
- The double-sided Howard policy iteration scheme is used for solving the max–min problem.
- An adaptive finite element formulation is used to resolve the interfaces between void and full material.
- The derivation of the stationarity conditions for the objective functional is outlined in detail.

Abstract

A phase-field based topology optimization approach is considered for the maximum stiffness or minimum compliance problem. The objective functional to be minimized consists in addition to the compliance a cost for gray solutions and a cost for interfaces between void and full material. Since the interfaces between void and full material are penalized via a volume integral in the original phase-field formulation there is no penalty associated with interfaces along the external boundaries. In the present contribution, an additional term representing the cost of interfaces at external boundaries is added to the functional subject to minimization. It is shown that the new boundary term enters the optimization as a Robin boundary condition. The method is implemented in a finite element setting and numerical simulations of typical structures are considered. The results indicate that the optimal designs are influenced by the cost of interfaces to a large extent.

Keywords: Topology optimization; Phase-field; Boundary energy; Double obstacle problem; Howard's algorithm

1. Introduction

Topology optimization has over the past decades qualified as an important tool in the design process. The method has evolved and the number of applications is vast, cf. [1,2] for an overview of the method and its applications. The objective of the optimization is in the present work to find a design that maximizes the stiffness for a given amount of material. The advantage of using the stiffness as the objective, or rather its complement the compliance, is that it is a

* Corresponding author.
E-mail address: mathias.wallin@solid.lth.se (M. Wallin).

http://dx.doi.org/10.1016/j.cma.2014.05.012
0045-7825/

global measure and thus can be represented by a scalar value. Moreover, the constraint on the volume is also particular simple since it is linear and monotone which in most cases gives rise to a robust numerical algorithm.

The most widely used numerical scheme for topology optimization is the Solid Isotropic Material with Penalization (SIMP) scheme where the density is approximated as constant within each element. The SIMP procedure is based on a sequence of convex approximations and the algorithm is simple to implement and at the same time numerically efficient. A distinct black/white solution is obtained by penalizing gray designs via a scaling of the elastic constitutive relation. This formulation has been shown to be ill-posed due to the length scale missing in the formulation, cf. e.g. [3]. A mesh-dependent solution can, however, be obtained, by using the finite element method where a length scale enters the formulation via the mesh size. However, to resolve the boundary a very fine or an adaptive mesh is needed, cf. e.g. [4].

Regularization of the topology optimization problem implies that a length scale is introduced in the problem formulation which removes the mesh dependency otherwise present in a finite element solution. Several procedures for regularization of the topology optimization problem has been proposed, these can be local such that the smallest size of a segment is limited, or it can restrict the total length of the perimeter. Such methods are known as filtering techniques [5], perimeter control, [6], gradient control [7,8] and recently also phase-field approaches [9,10]. All these methods has in common that they introduce a length scale in the formulation and thus restricting the smallest characteristic size either locally or globally.

The gradient control method, [7], has been shown to yield similar results as the filter based schemes. The drawback of the gradient control based method is that it implies a large number of additional constraints. The most frequent approach for regularizing the problem is to make use of the filter approach as proposed by [5,11] and further developed in e.g. [12]. A summary of filtering techniques can also be found in [13]. The filter approach is similar to the gradient control method, a local method, however compared to the gradient control method it is associated with a less computational cost. The original filter method is based on that a filtered sensitivity of the density, ρ, is used in the constitutive relation instead of the local density sensitivity. A typical filter can be described as

$$\xi^*(\boldsymbol{x}) = \int_{\Omega_c} \phi(\boldsymbol{x}-\boldsymbol{y})\xi(\boldsymbol{y})dV \tag{1}$$

where the filter function $\phi \geq 0$ fulfills the normalization condition $\int_{\Omega_c} \phi(\boldsymbol{x}-\boldsymbol{y})dV = 1$, Ω_c is a domain in $\mathbb{R}^d$, $d \in [2,3]$ with compact support. The filter is typically applied directly on the density field or on the sensitivity of the density. Several possibilities for the filter function, ϕ exists and the two most frequently employed filters are the linear and the Gaussian, bell-shaped, cf. e.g. [11,14].

The filter strategy is numerically simple to implement but the treatment of the boundaries deserves additional attention. The difficulties at the boundaries stems from the fact that the filter function, ϕ is defined over Ω_c which close to the boundary stretches outside the design domain, Ω. As a consequence, close to the boundaries of the design domain, $\partial\Omega$, the convolution (1) will involve values of the quantity, ξ, located outside the design domain, Ω. Assuming no material outside Ω and using (1) will inherently lead to a diffuse designs along design boundaries. One remedy (cf. e.g. [15]) is to exclude the part of Ω_c outside Ω along with a scaling of the filter function, ϕ. This procedure tends, however, to yield high values of the density at the interface. In contrast to modifying the filter function, the density field can be extended to the entire, Ω_c, by making use of symmetries. However, all the remedies mentioned above are suffering from having an unclear interpretation at the boundaries.

Another method for regularizing the stiffness problem was proposed in [6] where the objective functional is augmented such that the total variation (TV) of the density field is penalized. The total variation is related to the perimeter of the structure and defined as

$$\mathrm{TV} = \int_{\Omega\setminus\Gamma_j} |\nabla\rho| dV + \int_{\Gamma_j} |\langle\rho\rangle| dS \tag{2}$$

where the element boundaries are defined by Γ_j and $\langle\rangle$ represents the jump function. Since the absolute sign in (2) is non-differentiable at the origin, the problem is regularized using the smoothing functions, g and j, i.e.

$$P = \int_{\Omega\setminus\Gamma_j} g(|\nabla\rho|) dV + \int_{\Gamma_j} j(\langle\rho\rangle) dS. \tag{3}$$

In this approach, the finite element interpolations for the density field is chosen as piece-wise constant within each element such that jumps are allowed over the element boundaries as well as along the outer boundary. The functional P is then used for controlling the perimeter in the topology optimization problem. Penalization of material along the design domain boundaries can easily be included in the perimeter control scheme since the integral of the jump function, if elements with material is present, is taken over the design domain boundary. In contrast to the filter approach the method is global and can thus not be expected to strictly suppress very thin members locally.

Yet an alternative method for regularizing the stiffness problem is provided by the phase-field method, cf. [9,16]. The phase-field method was originally developed for simulation of evolution of micro-structural phenomena, cf. [17]. The energy, or cost term, related to interfaces is given by

$$\int_{\Omega} |\nabla \rho|^2 dV. \tag{4}$$

A comparison of the perimeter control scheme and the phase-field approach reveals that the two methods share some features. Both methods are penalizing gradients of the density field. In contrast to the perimeter control scheme the phase-field approach is based on a continuous density field which eliminates the need for penalization of interfaces between elements. However, from (4), it follows that there is no cost for material along the design domain boundaries, e.g. where regions with full material are located along the design boundary, and where $\nabla \rho = \mathbf{0}$. In the phase-field approach homogeneous Neumann boundary condition

$$\nabla \rho \cdot \boldsymbol{n} = 0 \quad \text{along } \partial \Omega \tag{5}$$

is imposed for the density field. The boundary condition (5) will enforce that the design is perpendicular to the design domain, cf. e.g. [10,16,18].

In conclusion, interfaces are penalized via a volume integral of square of the magnitude of the gradient of the density field, cf. (4), along with the boundary condition (5) in the phase-field approach. The boundary condition (5) implies that there is no cost for interfaces along the design domain boundary, this favors material along the design domain boundary. For most applications this feature is in conflict with the optimal design and in the present work a remedy to the problem is presented.

The phase-field approach employed in [18] is used as a basis in the present work. To introduce a cost for interfaces along the design domain, the objective functional in the present work is augmented with a boundary term which introduces a cost for creating external design boundaries. The derivations following the requirement of stationarity of the objective functional reveals that the new term in the objective functional can be interpreted as a Robin boundary condition (mixed boundary condition) for the density field along the design domain boundaries. The paper is closed by two simple examples where the effect of the new boundary term is demonstrated.

2. Preliminaries

The design space in which the structure is embedded is denoted $\Omega \subset \mathbb{R}^d$ of dimension $d = 2, 3$. The density, $\rho : \Omega \to [-1, 1]$, is taken as the design variable and void material is represented by $\rho = -1$ and full material is defined by $\rho = 1$. The total amount of material available for the design is given by, $\bar{V}$, i.e.

$$\bar{V} = \frac{1}{2}\left(\int_{\Omega} \rho \, dV + V_o\right) \tag{6}$$

where V_o is the volume of the design domain, Ω. The constitutive relation for the stress, $\boldsymbol{\sigma}$ is given as

$$\boldsymbol{\sigma}(\rho, \boldsymbol{u}) = \boldsymbol{D}(\rho) : \boldsymbol{\epsilon}(\boldsymbol{u}) \tag{7}$$

where the strain, $\boldsymbol{\epsilon}(\boldsymbol{u})$, is defined as the symmetric part of the gradient of the displacement field, $\boldsymbol{\epsilon}(\boldsymbol{u}) = (\nabla \boldsymbol{u})_{\text{sym}}$, where subscript sym denotes the symmetric part of the quantity, and $\boldsymbol{D}(\rho)$ represents the elastic stiffness tensor. Decreasing the density, ρ, will lead to a reduction of the stiffness. This relation, not necessarily linear, will here be used in a similar manner as in the SIMP method. Assuming the existence of a monotone function $g(\rho) : \mathbb{R} \to \mathbb{R}^+$, the stiffness of the material is described by $\boldsymbol{D} = g(\rho)\boldsymbol{D}_0$ where $\boldsymbol{D}_0$ represents the stiffness of the full material, i.e. $\rho = 1$. Void material is represented by $\rho = -1$ and it will later on be assumed that a residual stiffness is present for void material, i.e. $g(-1) = \epsilon_s^2 > 0$.

In absence of body forces and given density field, ρ, the strong form of the elastic equilibrium problem consist of finding the displacement $\boldsymbol{u}$ such that:

$$\begin{aligned} &\boldsymbol{\nabla}\cdot\boldsymbol{\sigma}(\rho,\boldsymbol{u})=\boldsymbol{0} \quad \text{in } \Omega \\ &\boldsymbol{u}=\boldsymbol{0} \quad \text{on } \partial\Omega_{D_u} \\ &\boldsymbol{\sigma}(\rho,\boldsymbol{u})\cdot\boldsymbol{n}=\boldsymbol{t}_o \quad \text{on } \partial\Omega_{N_u} \end{aligned} \tag{8}$$

where the boundary, $\partial\Omega$, is separated into $\partial\Omega = \partial\Omega_{N_u} \cup \partial\Omega_{D_u}$ and $\partial\Omega_{N_u} \cap \partial\Omega_{D_u} = \varnothing$ and where $\partial\Omega_{D_u}$ is the Dirichlet part where the displacement condition is imposed, and $\partial\Omega_{N_u}$ is the Neumann part where the surface traction $\boldsymbol{t}_o$ is applied. The outward unit vector normal to $\partial\Omega_{N_u}$ is denoted $\boldsymbol{n}$.

The variational (weak) form of the elastic problem is found by introducing the function space $\mathcal{V} := \{\bar{\boldsymbol{u}} \in [H^1(\Omega)]^d : \bar{\boldsymbol{u}}|_{\partial\Omega_{D_u}} = \boldsymbol{0}\}$. For given density distribution $\rho \in L^\infty(\Omega)$, find $\boldsymbol{u} \in \mathcal{V}$ such that:

$$V_u(\rho,\boldsymbol{u};\bar{\boldsymbol{u}}) = 0 \quad \forall\bar{\boldsymbol{u}} \in \mathcal{V} \tag{9}$$

where

$$V_u(\rho,\boldsymbol{u};\bar{\boldsymbol{u}}) = \int_\Omega \boldsymbol{\sigma}(\rho,\boldsymbol{u}) : \boldsymbol{\epsilon}(\bar{\mathbf{u}})dV - \int_{\partial\Omega_{N_u}} \boldsymbol{t_o}\cdot\bar{\boldsymbol{u}}dS. \tag{10}$$

It is noted that the solution $\boldsymbol{u}$ in (9) is obtained for a given density field ρ, i.e. the solution depends on the density distribution such that $\boldsymbol{u}(\rho)$.

3. Boundary augmented functional

The objective of the optimization is for fixed amount of material to find a distinct design that maximizes the stiffness of the structure. The stiffness of the structure is maximized when the compliance, C, defined as

$$\int_{\partial\Omega_t} \boldsymbol{t}_0\cdot\boldsymbol{u}dS = 2\int_\Omega w(\rho,\boldsymbol{u})dV = C(\rho,\boldsymbol{u}) \tag{11}$$

is taking a minimum value. Note that the elastic boundary value problem was used in the derivation of (11). In (11) $w(\rho,\boldsymbol{u}) = \frac{1}{2}\boldsymbol{\epsilon}(\boldsymbol{u}) : \boldsymbol{\sigma}(\rho,\boldsymbol{u})$ represents the specific strain energy. Although most phase-field studies have been concerned with the stiffness optimization problem it can be applied to other problems. In [19] local stress constraints was incorporated in a phase-field approach and in [20] it was shown that the phase-field based topology optimization scheme can be applied to minimal displacement problems. Intermediate, or gray, densities, $\rho \in \,]-1,1[$ are penalized via the penalization function, $F(\rho) : \mathbb{R} \to \mathbb{R}_o^+$ (subscript o indicates that zero is included in the set) and the total penalization for gray densities is given by

$$\int_\Omega F(\rho)dV \geq 0. \tag{12}$$

The penalty function $F(\rho)$ is frequently referred to as a double-well potential function or an obstacle potential function with the property $F(-1) = F(1) = 0$. Minimizing the compliance, C, using the penalization (12) will, similar to the SIMP scheme, result in a mesh-dependent solution due to a lacking length scale. To overcome this deficiency, the problem will be regularized using a phase-field approach which implies that a cost for gradients is included in the objective functional, see also the previous discussion in the introduction part and [21]. To summarize, the objective functional to be minimized will take the following format

$$\tilde{E}(\rho,\boldsymbol{u}) = \int_\Omega \left(F(\rho) + \frac{\gamma_1}{2}|\boldsymbol{\nabla}\rho|^2\right)dV + \eta C(\rho,\boldsymbol{u}) \tag{13}$$

where the influence of the compliance is governed by η and where $\boldsymbol{u} \in \mathcal{V}$ and $\rho \in \mathcal{M}$ with the space $\mathcal{M} := \{\bar{\rho} \in H^1(\Omega) : \bar{\rho}|_{\partial\Omega_{D_\rho}} = \rho_{D_\rho}\}$ where ρ_{D_ρ} is the prescribed density along $\partial\Omega_{D_\rho}$. The boundary for the density field ρ is then split according to $\partial\Omega = \partial\Omega_{N_\rho} \cup \partial\Omega_{D_\rho}$ and $\partial\Omega_{N_\rho} \cap \partial\Omega_{D_\rho} = \varnothing$. The second term in (13) represents the interface energy or gradient energy and the third term is not present in the micro-structural phase-field formulation and represents the

compliance which is subject to minimization. The functional (13) has previously been considered for topology optimization, cf. e.g. [21]. As discussed in the introduction, the solution obtained by minimization of (13) results in that interfaces located along the design domain boundary, $\partial\Omega$ are not penalized. As a consequence of lacking cost for interfaces along design boundaries it is favorable for material to be located along $\partial\Omega$. To include interface cost along $\partial\Omega$ the functional in (13) is augmented with an additional boundary term. The boundary of Ω will for the density problem now be split into $\partial\Omega = \partial\Omega_{R_\rho} \cup \partial\Omega_{D_\rho}$ and $\partial\Omega_{R_\rho} \cap \partial\Omega_{D_\rho} = \varnothing$, where R_ρ and D_ρ refers to Robin and Dirichlet boundary conditions, respectively. Using this split the objective functional $E(\rho, \boldsymbol{u})$, subject to minimization is given by

$$E(\rho, \boldsymbol{u}) = \int_\Omega \left(F(\rho) + \frac{\gamma_1}{2} |\nabla\rho|^2 \right) dV + \eta C(\rho, \boldsymbol{u}) + \frac{\gamma_2}{2} \int_{\partial\Omega_{R_\rho}} (\rho + 1)^2 dS. \tag{14}$$

The boundary integral proposed in (14) implies that a density not being void along $\partial\Omega_{R_\rho}$ contributes to the functional, E. The parameter γ_2 sets the cost for interfaces along the design domain. It is concluded that for $\rho = -1$, there is no cost for interfaces along $\partial\Omega_{R_\rho}$ whereas $\rho = 1$ implies a penalty of $2\gamma_2$ per unit length of the boundary. Note that for $\gamma_2 = 0$ the cost for material along the outer boundary vanishes and the usual homogeneous Neumann boundary condition used in the standard phase-field approach is recovered. Another special case is obtained by letting $\gamma_2 \to \infty$. From (14) it can be concluded that increasing γ_2 will force the density along $\partial\Omega_{R_\rho}$ to approach void material, i.e. a Dirichlet boundary condition is approached.

To satisfy, equilibrium, traction boundary conditions and volume constraint the objective functional is augmented such that the Lagrangian ψ is obtained, i.e.

$$\begin{aligned} \psi(\rho, \boldsymbol{u}, \boldsymbol{\lambda}^e, \boldsymbol{\lambda}^\rho) = E(\rho, \boldsymbol{u}) &+ \int_\Omega \boldsymbol{\lambda}^e \cdot \boldsymbol{\nabla} \cdot \boldsymbol{\sigma}(\boldsymbol{u}, \rho) dV + \lambda^\rho \left(\int_\Omega \rho dV + V_o - 2\bar{V} \right) \\ &+ \int_{\partial\Omega_{N_u}} \boldsymbol{\lambda}^t \cdot (\boldsymbol{t}^0 - \boldsymbol{\sigma}(\boldsymbol{u}, \rho) \cdot \boldsymbol{n}) dS \end{aligned} \tag{15}$$

where $\boldsymbol{u} \in \mathcal{V}$, $\rho \in \mathcal{M}$. The Lagrangian multipliers $\boldsymbol{\lambda}^e \in \mathcal{V}$ and $\boldsymbol{\lambda}^t \in \mathcal{V}$ are enforcing equilibrium and traction boundary condition, respectively. Finally, $\lambda^\rho \in \mathbb{R}$ is a Lagrangian multiplier enforcing the volume constraint.

3.1. Stationarity

An optimal state is characterized by its Lagrangian (15) being stationary. Taking advantage of that the stresses can be derived from the strain energy as

$$\boldsymbol{\sigma} = w_{,\boldsymbol{\varepsilon}} \tag{16}$$

allows the first variation of the objective functional to be written as

$$\begin{aligned} \delta\psi = &\int_\Omega \left(F_{,\rho} - \gamma_1 \Delta\rho - \boldsymbol{\nabla}\boldsymbol{\lambda}^e : w_{,\boldsymbol{\varepsilon}\rho} + 2\eta w_{,\rho} + \lambda^\rho \right) \delta\rho \, dV + \int_{\partial\Omega_{N_\rho} \cap \partial\Omega_{N_u}} \left(\boldsymbol{\lambda}^e - \boldsymbol{\lambda}^t \right) \cdot w_{,\boldsymbol{\varepsilon}\rho} \cdot \boldsymbol{n} \, \delta\rho \, dS \\ &+ \int_\Omega \left(2\eta w_{,\boldsymbol{\varepsilon}} - \boldsymbol{\nabla}\boldsymbol{\lambda}^e : w_{,\boldsymbol{\varepsilon}\boldsymbol{\varepsilon}} \right) : \boldsymbol{\varepsilon}(\delta\boldsymbol{u}) \, dV + \int_{\partial\Omega_{N_u}} \left(\boldsymbol{\lambda}^e - \boldsymbol{\lambda}^t \right) \cdot \left(w_{,\boldsymbol{\varepsilon}\boldsymbol{\varepsilon}} : \boldsymbol{\varepsilon}(\delta\boldsymbol{u}) \right) \cdot \boldsymbol{n} \, dS \\ &+ \gamma_2 \int_{\partial\Omega_{R_\rho}} (\rho + 1) \delta\rho \, dS + \gamma_1 \int_{\partial\Omega_{R_\rho}} \boldsymbol{\nabla}\rho \cdot \boldsymbol{n} \delta\rho \, dS = 0 \quad \forall \, \delta\boldsymbol{u} \in \mathcal{V}, \ \delta\rho \in \mathcal{K} \end{aligned} \tag{17}$$

where $\mathcal{K} := \{\bar{\rho} \in H^1(\Omega) : \bar{\rho}|_{\partial\Omega_{D_\rho}} = 0\}$.

Let us first consider the two last boundary integrals in (17). To satisfy stationarity of (17) a mixed, Robin type, boundary condition for $\boldsymbol{\rho} \cdot \boldsymbol{n} = 0$ is assumed

$$\gamma_1 \boldsymbol{\nabla}\rho \cdot \boldsymbol{n} = -\gamma_2 (1 + \rho) \quad \text{along } \partial\Omega_{R_\rho}. \tag{18}$$

The boundary condition (18) implies that the two last surface integrals in (17) vanish. Next, following [18] where it is shown that $\boldsymbol{\lambda}^e = \boldsymbol{\lambda}^t = 2\eta\boldsymbol{u}$ results in the reduced functional

$$\delta\psi = \int_\Omega \left(F_{,\rho} - \gamma_1 \Delta\rho + \lambda^\rho - 2\eta \frac{g_{,\rho}}{g} w \right) \delta\rho dV = 0 \quad \forall \, \delta\rho \in \mathcal{M} \tag{19}$$

where it was used that $w_{,\rho} = g_{,\rho}\boldsymbol{\epsilon} : \boldsymbol{D}_o : \boldsymbol{\epsilon} = \frac{g_{,\rho}}{g} w$. By localization the optimality criteria can be expressed, find ρ subjected to (8) and (6) such that:

$$\begin{aligned} &F_{,\rho} - \gamma_1 \Delta\rho + \lambda^\rho - 2\eta \frac{g_{,\rho}}{g} w = 0 \quad \text{in } \Omega \\ &\rho = 0 \quad \text{along } \partial\Omega_{D_\rho} \\ &\gamma_1 \nabla\rho \cdot \boldsymbol{n} = -\gamma_2(1+\rho) \quad \text{along } \partial\Omega_{R_\rho}. \end{aligned} \tag{20}$$

The variational (weak) form of the optimality criteria is given as, find $\rho \in \mathcal{M}$ subjected to (9) and (6) such that

$$\bar{V}_\rho(\boldsymbol{u}, \rho, \lambda^\rho; \bar{\rho}) = 0 \quad \forall \bar{\rho} \in \mathcal{M} \tag{21}$$

where

$$\begin{aligned} \bar{V}_\rho(\boldsymbol{u}, \rho, \lambda^\rho; \bar{\rho}) = &\int_\Omega \bar{\rho} F_{,\rho} dV + \int_{\partial\Omega_{N_\rho}} \gamma_2 \bar{\rho}(1+\rho)\, dS + \int_\Omega \gamma_1 \nabla\bar{\rho} \cdot \nabla\rho dV \\ &+ \int_\Omega \bar{\rho}\lambda^\rho dV - \int_\Omega 2\eta\bar{\rho} w_{,\rho} dV \end{aligned} \tag{22}$$

where the coupling to the mechanical field (9) enters via $w_{,\rho}$.

4. Specific formats

Several possible formats for the cost function, F and the elastic scaling function g exist. In [18] use was made of a smooth functions F with high penalty for ρ outside the range $[-1, 1]$. Too high penalty in that formulation will affect the numerical algorithm and lead to convergence problems. A continuous penalty function F do not strictly exclude densities above the upper limit thus false stiffness could be the outcome. However, this problem can be avoided by use of a cut-off for g at $\rho = 1$, cf. e.g. [22]. This approach would also influence upon the interpretation of the volume constraint since areas where $|\rho| > 1$ can exist. An alternative route was employed in [23,21] where a non-smooth obstacle potential function was utilized. This approach will be employed in the present formulation. For this situation the penalization function, F will take the format

$$F(\rho) = I(\rho) + F_0(\rho) \tag{23}$$

where $F_0(\rho) = (1 - \rho^2)/2$ and where the indicator function, I, is defined as

$$I_{[-1,1]}(\rho) = \begin{cases} 0 & \rho \in [-1, 1] \\ \infty & \text{otherwise.} \end{cases} \tag{24}$$

The choice (23) will result in infinite penalty for densities $\rho \notin [-1, 1]$ which implies that the local density will not violate the constraint $\rho \in [-1, 1]$. The derivative of F enters optimality criteria (20) and for the situation where F is non-smooth deserves extra consideration. Using the concept of subderivative the derivative of F can be expressed as

$$F_{,\rho} = F_{0,\rho} + \mu \tag{25}$$

where μ is in the subdifferential of I which is the normal cone $N_{[-1,1]}(\rho)$ to $[-1, 1]$, and has the properties

$$\mu \in \partial I_{[-1,1]}(\rho) = N_{[-1,1]}(\rho) = \begin{cases} (-\infty, 0], & \rho = -1 \\ 0 & \rho \in (-1, 1) \\ [0, \infty) & \rho = 1. \end{cases} \tag{26}$$

The choice (26) gives rise to an extra complication due to the non-smoothness and that μ for $\rho = 1$ and -1 is an unknown quantity. The solution to this problem will be discussed together with the definition of the max–min problem and Howard's policy iteration scheme. For this purpose let us define the following sets

$$\begin{aligned} &A^+ = \{\boldsymbol{x} \in \Omega \mid \rho = 1\} && \text{Upper coincidence set} \\ &A^- = \{\boldsymbol{x} \in \Omega \mid \rho = -1\} && \text{Lower coincidence set} \\ &A = A^+ \cup A^- && \text{Coincidence set} \\ &N = \{\boldsymbol{x} \in \Omega \mid -1 < \rho < 1\} && \text{Non-coincidence set.} \end{aligned} \tag{27}$$

These sets turn out to be useful later when the max–min problem will be formulated.

The scaling function g used in the stiffness is in the present work chosen as

$$g(\rho) = (1 + \rho + \epsilon_s)^2/4 \tag{28}$$

where the threshold value is taken as $\epsilon_s = 10^{-5}$ in the numerical examples. The choice (28) sets the residual stiffness as ϵ_s^2 times the nominal stiffness and this choice ensures that the elastic problem is non-singular.

5. Phase-field approach

In order for the solution to evolve towards a minimum of the objective functional, the non-conserving Ginzburg–Landau also known as the Allen–Cahn approach is used for defining the set of evolution laws for the system. This approach will guarantee that the objective functional will approach a minimum. However due to the non-convexity of the system a stationary point cannot be guaranteed to be a global minimum.

To find a state that fulfills (20)a a steepest decent approach will be adopted. The search direction is the residual of (20)a and the solution is allowed to evolve until (20)a is fulfilled within a given tolerance. In conclusion, the rate of change of the density distribution, $-\dot{\rho}$ is taken to be proportional to the left hand side of (20)a, i.e.

$$-\gamma_1 \dot{\rho} = F_{,\rho} - \gamma_1 \Delta\rho + \lambda^\rho - 2\eta w_{,\rho}. \tag{29}$$

Then from (19), considering the time rate instead of variation, by the use of (29) it then immediately follows that

$$\dot{\psi} = -\gamma_1 \int_\Omega (-F_{,\rho} + \gamma_1 \Delta\rho - \lambda^\rho + 2\eta w_{,\rho})^2 \leq 0 \tag{30}$$

i.e. a minimum of ψ is approached for the evolution law (29).

5.1. Time discretization

Before the finite element formulation is discussed, a time discretization for the density field is introduced. Here, the backward-Euler approximation for $\dot{\rho}$ will be employed, i.e.

$$\dot{\rho} = \frac{\rho - \rho^n}{\tau} \tag{31}$$

where τ is the time elapsed during the time-step and ρ^n is the known density at time t_n. For the present problem, the time step has no physical meaning and it will be chosen such that convergence is obtained. Insertion of (31) into (29) and using (25) yields

$$\frac{\gamma_1}{\tau}(\rho - \rho^n) + F_{0,\rho} - \gamma_1 \Delta\rho + \lambda^\rho - 2\eta w_{,\rho} = -\mu. \tag{32}$$

Taking advantage of (26) it follows that instead of (32) a max–min problem can be stated. However, let us first recall some preliminary results:

$$\begin{aligned}
&\frac{\gamma_1}{\tau}(\rho - \rho^n) + F_{0,\rho} - \gamma_1 \Delta\rho + \lambda^\rho - 2\eta w_{,\rho} \geq 0 \quad \text{in } A^- \\
&\frac{\gamma_1}{\tau}(\rho - \rho^n) + F_{0,\rho} - \gamma_1 \Delta\rho + \lambda^\rho - 2\eta w_{,\rho} = 0 \quad \text{in } N \\
&\frac{\gamma_1}{\tau}(\rho - \rho^n) + F_{0,\rho} - \gamma_1 \Delta\rho + \lambda^\rho - 2\eta w_{,\rho} \leq 0 \quad \text{in } A^+ \\
&\rho - 1 \leq 0 \quad \text{in } \Omega \\
&\rho + 1 \geq 0 \quad \text{in } \Omega.
\end{aligned} \tag{33}$$

The split in (33) into the different sets implies that μ is not evaluated explicitly. Instead a selection procedure is introduced such that the correct equation is used from the material point at hand, i.e. a selection between (33)b, d and e. For this selection procedure, Howard's policy iteration scheme will be introduced in the sequel. Also for this purpose it is concluded that the inequalities in (33) can be stated as a max–min problem

$$\max\left(\min\left(\frac{\gamma_1}{\tau}(\rho - \rho^n) + F_{0,\rho} - \gamma_1 \Delta\rho + \lambda^\rho - 2\eta w_{,\rho}, \rho + 1\right), \rho - 1\right) = 0 \quad \text{in } \Omega \tag{34}$$

which describes the problem at hand. This statement must, evidently, be supplemented with the volume constraint and the elastic problem.

With the above at hand, the variational (weak) forms of the time discretized evolution equation of the density field and the associated elastic problem can be stated where advantage is taken of the sets defined in (27). Find $\boldsymbol{u} \in \mathcal{V}$, $\rho \in \mathcal{M}$, $\mu \in N_{[-1,1]}(\rho)$ and $\lambda^\rho \in \mathbb{R}$ in Ω such that:

$$\begin{aligned} &V_u(\rho, \boldsymbol{u}, \bar{\boldsymbol{u}}) = 0 \quad \forall\, \bar{\boldsymbol{u}} \in \mathcal{V} \\ &V_\rho(\bar{\rho}, \boldsymbol{u}, \lambda^\rho, \mu, \rho) = 0 \quad \forall\, \bar{\rho} \in \mathcal{M} \\ &C_1(\rho) = \rho - 1 \leq 0 \\ &C_2(\rho) = \rho + 1 \geq 0 \\ &C_3(\rho) = \int_\Omega \rho \, dV + V_o - 2\bar{V} = 0 \end{aligned} \tag{35}$$

where

$$\begin{aligned} V_\rho(\boldsymbol{u}, \rho, \lambda^\rho, \mu; \bar{\rho}) = &\int_\Omega \bar{\rho} F_{o,\rho} dV + \int_\Omega \bar{\rho}\mu \, dV + \int_{\partial\Omega_{N_\rho}} \gamma_2 \bar{\rho}(1+\rho)\, dS \\ &+ \int_\Omega \gamma_1 \boldsymbol{\nabla}\rho \cdot \boldsymbol{\nabla}\bar{\rho} dV + \int_\Omega \bar{\rho}\lambda^\rho dV - \int_\Omega 2\eta\bar{\rho} w_{,\rho} dV. \end{aligned} \tag{36}$$

6. Finite element setting

The computational domain Ω is approximated by $\bar{\Omega}$ which consists of the set of elements $\mathcal{T}_h$ such that $\bar{\Omega} = \cup_{K\in\mathcal{T}_h} K$. The finite element spaces used for the displacement and the density field consist of piece-wise mth order polynomials, P_m, with $m \geq 1$, i.e.

$$\begin{aligned} \mathcal{V}^h &= \left\{ \bar{\boldsymbol{u}}_h \in H^1(\bar{\Omega});\ \bar{\boldsymbol{u}}_{h|K} \in P_m(K),\ \forall K \in \mathcal{T}_h,\ \ \bar{\boldsymbol{u}}_h|_{\partial\Omega_{D_u}} = \boldsymbol{0} \right\} \\ \mathcal{M}^h &= \left\{ \bar{\rho}_h \in H^1(\bar{\Omega});\ \bar{\rho}_{h|K} \in P_m(K),\ \forall K \in \mathcal{T}_h,\ \ \bar{\rho}_h|_{\partial\Omega_{D_\rho}} = 0 \right\}. \end{aligned} \tag{37}$$

The finite element space for the subdifferential of the indicator function is taken as

$$\mathcal{W}^h = \left\{ v_h \in \sum_n \delta(\boldsymbol{x} - \boldsymbol{x}_n)\alpha_n;\ \alpha_n \in \mathbb{R};\ \boldsymbol{x}_n \in \bar{\Omega} \right\} \tag{38}$$

where δ denotes the Dirac delta function and where the collocation points $\boldsymbol{x}_n$ are chosen to coincide with the finite element nodal points. This choice is sufficient for our purposes and it will later on be shown to be compatible with the numerical scheme.

The solution to the finite element problem can then with the use of (37) and (38) be stated as, find $\boldsymbol{u}_h \in \mathcal{V}^h$, $\rho_h \in \mathcal{M}^h$, $\mu_h \in \mathcal{W}^h$ and $\lambda^\rho \in \mathbb{R}$ in Ω such that

$$\begin{aligned} &V_u^h(\rho_h, \boldsymbol{u}_h, \bar{\boldsymbol{u}}_h) = 0 \quad \forall\, \bar{\boldsymbol{u}}_h \in \mathcal{V}^h \\ &V_\rho^h(\rho_h, \boldsymbol{u}_h, \lambda^\rho, \mu_h, \bar{\rho}_h) = 0 \quad \forall\, \bar{\rho}_h \in \mathcal{M}^h \\ &C_1(\rho_h) = \rho_h - 1 \leq 0 \\ &C_2(\rho_h) = \rho_h + 1 \geq 0 \\ &C_3(\rho_h) = \int_{\bar{\Omega}} \rho_h \, dV + V_o - 2\bar{V} = 0 \end{aligned} \tag{39}$$

is fulfilled.

To reduce the size of the resulting system a staggered time stepping procedure will here be employed, i.e. the equilibrium will be solved for fixed densities followed by an update of the density field for a fixed derivative of the strain energy, $w_{,\rho}$.

6.1. Solution strategy

It has been shown in [21] that a staggered approach is a feasible approach especially since the density problem is characterized as a non-smooth problem. In the staggered approach, first the elastic problem is solved for a given density field after this step the density field is solved using Howard's algorithm.

The solution procedure can formally be stated as

- For given $\rho_g = \rho_h$, find $\boldsymbol{u}_h \in \mathcal{V}^h$ such that

$$V_u(\boldsymbol{u}_h, \rho_g; \bar{\boldsymbol{u}}_h) = \boldsymbol{0} \quad \forall\, \bar{\boldsymbol{u}}_h \in \mathcal{V}^h. \tag{40}$$

- For given $\boldsymbol{u}_g = \boldsymbol{u}_h$ and function $g(\rho_h)$, find $\rho_h \in \mathcal{M}^h$, $\lambda^\rho \in \mathbb{R}$ and $\mu_h \in \mathcal{W}^h$ such that

$$\begin{aligned} &V_\rho^h(\rho_h, \boldsymbol{u}_g, \lambda^\rho, \mu_h, \bar{\rho}_h) = 0 \quad \forall\, \bar{\rho}_h \in \mathcal{M}^h \\ &C_1(\rho_h) = \rho_h - 1 \geq 0 \\ &C_2(\rho_h) = \rho_h + 1 \leq 0 \\ &C_3(\rho_h) = \int_{\bar{\Omega}} \rho_h \, dV + V_o - 2\bar{V} = 0. \end{aligned} \tag{41}$$

Note that the scaling function g given in (28) is taken to be constant in the second stage, together with fixed displacements corresponds to assuming that $w_{,\rho}$ is constant, i.e. a semi-implicit method is utilized.

The elastic problem is linear as it is solved for constant density field. This can be considered as a standard linear elastic problem and is therefore not discussed in detail here. Instead emphasis will be given to the non-smooth density problem which is solved using a double sided version of Howard's algorithm as introduced by [24]. Also the density problem needs some consideration since a selection must be done, cf. the continuous problem defined in (34). To derive the discrete counterpart part to (34), explicit matrix formats corresponding to V_ρ^h will be given. By denoting the matrix containing the shape functions $\boldsymbol{N}$ and the matrix containing the gradient of the shape functions $\boldsymbol{B}$ the following matrix format of (41)a is obtained

$$\left(\left(\frac{\gamma_1}{\tau} - 1\right)\boldsymbol{M} + \gamma_1 \boldsymbol{K}_0 + \gamma_2 \boldsymbol{K}_R\right)\boldsymbol{\rho} + \boldsymbol{P}\lambda^\rho - \frac{\gamma_1}{\tau}\boldsymbol{M}\boldsymbol{\rho}_n - 2\eta \int_{\bar{\Omega}} \boldsymbol{N}^T w_{,\rho} dV + \gamma_2 \boldsymbol{P}_R = -\boldsymbol{\mu} \tag{42}$$

where $\boldsymbol{\rho}$ and $\boldsymbol{\mu}$ denote the nodal values of ρ_h and μ_h, respectively. In (42), the following constant matrices were introduced

$$\boldsymbol{M} = \int_{\bar{\Omega}} \boldsymbol{N}^T \boldsymbol{N} dV, \qquad \boldsymbol{K}_0 = \int_{\bar{\Omega}} \boldsymbol{B}^T \boldsymbol{B} dV, \qquad \boldsymbol{P} = \int_{\bar{\Omega}} \boldsymbol{N}^T dV, \tag{43}$$

and

$$\boldsymbol{K}_R = \int_{\partial \bar{\Omega}_{R_\rho}} \boldsymbol{N}^T \boldsymbol{N} dS, \qquad \boldsymbol{P}_R = \int_{\partial \bar{\Omega}_{R_\rho}} \boldsymbol{N}^T dS. \tag{44}$$

Collecting the terms in (42) enable the system to be written in the compact format

$$\boldsymbol{A}\boldsymbol{\rho} + \boldsymbol{P}\lambda^\rho - \boldsymbol{b} = -\boldsymbol{\mu}. \tag{45}$$

It is also noted that the volume constraint, (41)d, can be written as

$$\boldsymbol{P}^T \boldsymbol{\rho} + V_o - 2\bar{V} = 0. \tag{46}$$

Since the function spaces as well as the domain is discretized it is advantageous to define the sets corresponding to (27), such that:

$$\begin{aligned} &A^{h+} = \{\boldsymbol{x} \in \bar{\Omega} \mid \rho_h = 1\} && \text{Upper coincidence set} \\ &A^{h-} = \{\boldsymbol{x} \in \bar{\Omega} \mid \rho_h = -1\} && \text{Lower coincidence set} \\ &A^h = A^{h+} \cup A^{h-} && \text{Coincidence set} \\ &N^h = \{\boldsymbol{x} \in \bar{\Omega} | -1 < \rho^h < 1\} && \text{Non-coincidence set.} \end{aligned} \tag{47}$$

Using the definition (26), three cases of (45) can be distinguished.

$$\begin{cases} \left\{\boldsymbol{A}\boldsymbol{\rho} + \boldsymbol{P}\lambda^{\rho} - \boldsymbol{b}\right\}_{\alpha} \geq 0 & \forall\, \boldsymbol{x}_{\alpha} \in A^{h+} \\ \left\{\boldsymbol{A}\boldsymbol{\rho} + \boldsymbol{P}\lambda^{\rho} - \boldsymbol{b}\right\}_{\alpha} = 0 & \forall\, \boldsymbol{x}_{\alpha} \in N^{h} \\ \left\{\boldsymbol{A}\boldsymbol{\rho} + \boldsymbol{P}\lambda^{\rho} - \boldsymbol{b}\right\}_{\alpha} \leq 0 & \forall\, \boldsymbol{x}_{\alpha} \in A^{h-} \end{cases} \tag{48}$$

where $\boldsymbol{x}_{\alpha}$ denotes the location of node α and where $\{\cdot\}_{\alpha}$ denotes the α row of the system. It is important to realize that the system (48) should be solved along with (46). It is easily verified that the three cases in (48) can be formulated as a max–min problem, i.e.

$$\begin{aligned} &\max(\min(\boldsymbol{A}\boldsymbol{\rho} + \boldsymbol{P}\lambda^{\rho} - \boldsymbol{b}, \boldsymbol{\rho} + \boldsymbol{1}), \boldsymbol{\rho} - \boldsymbol{1}) = \boldsymbol{0} \\ &\boldsymbol{P}^{T}\boldsymbol{\rho} + V_o - 2\bar{V} = 0. \end{aligned} \tag{49}$$

The min and max operators in (49) should be evaluated row-wise, i.e. for each row $\max(\min(\{\boldsymbol{A}\boldsymbol{\rho} + \boldsymbol{P}\lambda^{\rho} - \boldsymbol{b}\}_{\beta}, \{\boldsymbol{\rho} + \boldsymbol{1}\}_{\beta}), \{\boldsymbol{\rho} - \boldsymbol{1}\}_{\beta}) = 0$ should be evaluated. It is also noted that this is the max–min statement of the discrete problem corresponding to the continuous problem in (34). The max–min problem (49) is often referred to as a double obstacle problem where the upper and lower limits represents the obstacles. Several strategies for solving the problem (49) exists. In [25] the Primal Dual Active Set (PDAS) strategy was employed. In [21], this problem was solved using the Howard policy iteration scheme. The Howard policy iteration scheme will be used herein and it will therefore briefly be recaptured below.

6.1.1. Howard's policy iteration algorithm

As shown in [24], Howard's single obstacle solution procedure can be generalized to the double obstacle problem (49). Policy iteration schemes can be said to consist of a policy improvement and a policy evaluation. To formulate this consider first a template problem such as

$$\min(\boldsymbol{B}_1\boldsymbol{\rho} - \boldsymbol{c}_1,\ \boldsymbol{B}_2\boldsymbol{\rho} - \boldsymbol{c}_2) = \boldsymbol{0} \tag{50}$$

where $\boldsymbol{B}_i$ are $n \times n$ matrices and $\boldsymbol{\rho}$ and $\boldsymbol{c}_i$ are column matrices of size n. This statement corresponds to the single obstacle problem.

Next let us introduce a nonempty set compact set $\mathcal{A} = \{0\ 1\}$, and $\alpha \in \mathcal{A}^n$ which are called polices and n is the number of rows in the min statements. Note that n corresponds to the number of degrees of freedom in the system. The policy α then determines if the first or the second argument in (50) is the solution corresponding to $\alpha = 0$ and $\alpha = 1$, respectively. It should be noted that this selection procedure generates a new linear equation system. The introduction of polices allows for a more compact notation, namely

$$\min_{\alpha \in \mathcal{A}^n} (\boldsymbol{B}(\alpha)\boldsymbol{\rho} - \boldsymbol{c}(\alpha)) = \boldsymbol{0}. \tag{51}$$

With the above, the policy iteration scheme which computes a solution $\boldsymbol{\rho}^*$ from a sequence of trial values $\boldsymbol{\rho}^k$ and policies α^k can be defined as

$$\alpha^{k+1} = \arg \min_{\alpha \in \mathcal{A}^n} [\boldsymbol{B}(\alpha)\boldsymbol{\rho} - \boldsymbol{c}(\alpha)] \quad \text{(policy improvement)}$$

$$\boldsymbol{\rho}^{k+1} \text{is a solution of } \boldsymbol{B}(\alpha^{k+1})\boldsymbol{\rho} - \boldsymbol{c}(\alpha^{k+1}) = \boldsymbol{0} \quad \text{(policy evaluation)}.$$

With these preliminary results let us consider the max–min problem, i.e. the double obstacle problem. For the double obstacle problem two policies are used, one for each obstacle. Let $\mathcal{A}$ and $\mathcal{B}$ be two nonempty compact sets and let the policies associated with $\mathcal{A}$ and $\mathcal{B}$ be denoted $\alpha \in \mathcal{A}^n$ related to the min problem and $\beta \in \mathcal{B}^n$ related to the max problem. The max–min problem can then be stated as

$$\max_{\beta \in \mathcal{B}^n} \Big(\min_{\alpha \in \mathcal{A}^n} (\boldsymbol{B}(\alpha, \beta)\boldsymbol{\rho} - \boldsymbol{c}(\alpha, \beta)) \Big) = \boldsymbol{0} \tag{52}$$

i.e. the two policies will form a new linear equation system which fulfills the max–min condition. To be more explicit, the particular solution procedure based on (49) can be reformulated into

$$\boldsymbol{G}(\boldsymbol{\rho}) = \max_{\beta \in \mathcal{B}^n} \boldsymbol{Q}^{\beta}(\boldsymbol{\rho}) = \boldsymbol{0} \tag{53}$$

where the following definitions are used (the subscript i denotes the row)

$$\left\{\boldsymbol{Q}^{\beta}(\boldsymbol{\rho})\right\}_i = \begin{cases} \boldsymbol{F}^{\beta}(\boldsymbol{\rho})_i & \text{if } \beta_i = 0 \\ \{\boldsymbol{\rho}\}_i - 1 & \text{if } \beta_i = 1 \end{cases} \tag{54}$$

and using the notation above the min statement can be written as

$$\boldsymbol{F}^{\beta}(\rho) = \min_{\alpha \in \mathcal{A}^N} \left(\boldsymbol{B}(\alpha, \beta)\boldsymbol{\rho} - \boldsymbol{c}(\alpha, \beta)\right). \tag{55}$$

It is then concluded that the rows where the policy $\beta_i = 0$ is given as

$$\{\boldsymbol{B}(\alpha, \beta)\}_{ij} = \begin{cases} \{\boldsymbol{A}\}_{ij} & \text{if } \alpha_i = 0 \\ \delta_{ij} & \text{if } \alpha_i = 1 \end{cases} \quad \text{and} \quad \{\boldsymbol{c}(\alpha, \beta)\}_i = \begin{cases} \left\{\boldsymbol{b} - \boldsymbol{P}\lambda^{\rho}\right\}_i & \text{if } \alpha_i = 0 \\ -\{\boldsymbol{1}\}_i & \text{if } \alpha_i = 1. \end{cases} \tag{56}$$

Note that for rows where the policy $\beta_i = 1$ the row is given by the second choice in (54).

In the two-stage stage procedure by [24] the min problem is first solved for $\boldsymbol{\rho}$ with fixed policies β, i.e. $\boldsymbol{F}^{\beta}(\rho)$ then the max problem is solved for fixed policies α. The algorithm is outlined below

- Howard algorithm for a single obstacle: (For a fixed β^q)
  Iterate for $k \geq 0$
  (i) Find $\boldsymbol{\rho}^k$ such that $\boldsymbol{F}^{\beta^q}(\boldsymbol{\rho}^k) = \boldsymbol{B}(\alpha^k, \beta^q)\boldsymbol{\rho}^k - \boldsymbol{q}(\alpha^k, \beta^q) = \boldsymbol{0}$
  (ii) If $k \geq 1$ and $\boldsymbol{\rho}^k = \boldsymbol{\rho}^{k-1}$ stop
  (ii) Compute $\alpha^{k+1} := \arg\min_{\alpha \in \mathcal{A}^n} \boldsymbol{F}^{\beta}(\boldsymbol{\rho}^k)$
  (iii) Set $k := k + 1$ and go to (i).

For the particular system in question and the solution of (i) the policies results in that prescribed values on $\boldsymbol{\rho}$ are imposed. With the single obstacle algorithm at hand, the two stage algorithm can be written as

- Howard algorithm for double obstacles: (Initiate α^o and β^o)
  Iterate for $q \geq 0$
  (i) Find $\boldsymbol{\rho}^q$ such that $\boldsymbol{Q}^{\beta^q}(\boldsymbol{\rho}^q) = \boldsymbol{0}$ (solution given by Howard algorithm obstacle for fixed β^q)
  (ii) Compute $\beta^{q+1} := \arg\max_{\beta \in \mathcal{B}^n} \boldsymbol{Q}^{\beta}(\boldsymbol{\rho}^q)$
  (iii) If $\boldsymbol{G}(\boldsymbol{\rho}^q) = \boldsymbol{Q}^{\beta^{q+1}}(\boldsymbol{\rho}^q) = \boldsymbol{0}$ then stop;
  Else set $q := q + 1$ and go to (i).

It is important to realize that densities coinciding with the obstacles are not part of the linear system that should be solved, i.e. the size of the linear system that is required to be solved in each iteration is determined by the number of degrees of freedom in the diffuse interfaces.

7. Numerical examples

To illustrate the presented formulation and its numerical implementation, two boundary value problems will be considered. The geometries along with the boundary conditions are depicted in Fig. 1. The magnitude of the applied forces are chosen as 1. Plane stress and isotropy is assumed and the elastic parameters Young's modulus and Poisson's ratio are chosen to be 1 and 0.3, respectively. The dimensions of the design domains in the plane of loading are taken as 3×1 in Fig. 1(a) and 2×2 in Fig. 1(b). The elements used in the finite element simulation are linear triangular plane elements and to resolve the interface a mesh refinement strategy is employed. A hierarchical element refinement strategy is used. As the material density field only varies in the interfaces the refinement is concentrated to these areas, and since the range of the material density field is known and bounded a simple refinement rule can be adopted. The adaptivity is based on that if the difference in material density in an element is greater than 0.3 the element is refined and if the difference in the material density within an element is less than 0.01 the element will be coarsened if possible. This strategy will ensure that the interfaces are properly resolved. The initial mesh for the geometry in Fig. 1(a) consist of 660 elements and for the geometry in Fig. 1(b) of 800 elements.

The adaptive time stepping used in the examples below is based on the number of iterations used in the policy iteration scheme, i.e. no error estimation is used. If the total (inner and outer) iterations is less that 5 the time step is increases by 20% until the maximum time step $\tau_{\max} = 1 \cdot 10^{-4}$ is reached. The initial time step is taken as $\tau_{init} = 1 \cdot 10^{-8}$.

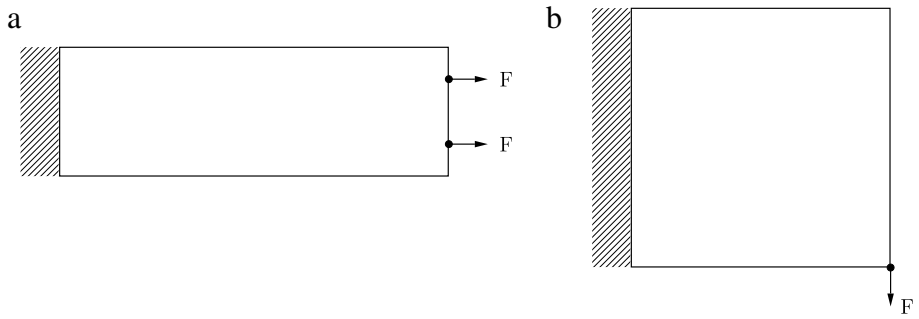

Fig. 1. Illustration of geometry and boundary conditions used in the numerical examples.

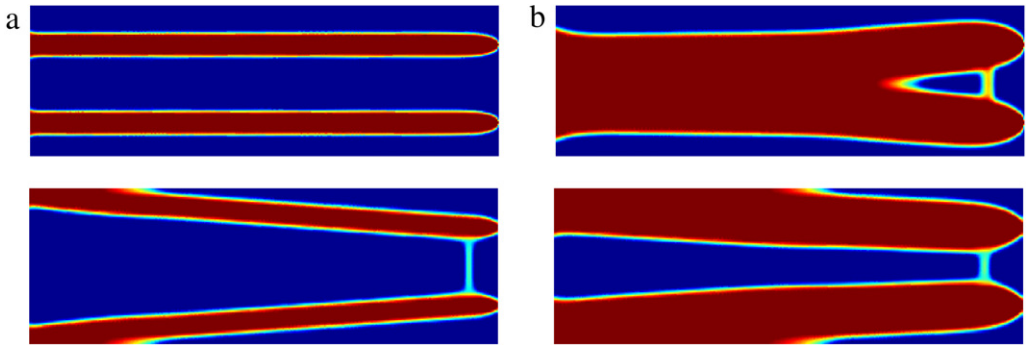

Fig. 2. The shapes of the optimal structures for material $\bar{V} = 0.3V_o$ for the two left figures and $\bar{V} = 0.65V_o$ for the two right figures and for the two lower figures $\gamma_2 = 0$ whereas for the two top figures $\gamma_2 = 100$. Blue color indicates void material and red full material. (For interpretation of the references to color in this figure legend, the reader is referred to the web version of this article.)

7.1. Bar structure

To illustrate the implication of the boundary term a first simple example is considered where two horizontal point loads, located $1/4$ from the top and bottom, are applied, cf. Fig. 1(a). Although this structure is very simple, it provides insight into the behavior of the boundary penalty term presented herein. On the left side homogeneous Dirichlet displacement boundary conditions are present. An initial homogeneous distribution of the material density is considered for which two different levels are used namely $\bar{V} = 0.3V_o$ corresponding to that the design domain is filled with 30% material and $\bar{V} = 0.65V_o$ which corresponds to that the design domain is filled with 65% material. The parameters $\gamma_1 = 0.5$ and $\eta = 200$ are used for the case of $\bar{V} = 0.3V_o$ and $\gamma_1 = 0.4$ and $\eta = 400$ for the case $\bar{V} = 0.65V_o$. The parameter controlling the boundary penalty are used, $\gamma_2 = 0$ and 100. The boundaries where the boundary penalty will be present are the top, bottom and right external boundaries, cf. Fig. 1(a), i.e. the boundary penalty is not present at the left boundary.

The results from the simulations are shown in Fig. 2. It is clearly seen that when the boundary penalty is absent, material tend to be located along the external boundaries as this is favorable. This optimized structure differ considerably from the situation when the boundary penalty term is present. For the situation without the boundary term it is also noted that a diffuse bridge is present between the two part. It is concluded that this bridge is present since it compensates for the fact that the two parts of the optimized structures are not horizontally aligned.

For the situation when the boundary penalty term is present it is noted that for small levels of total volume two bar like structures are obtained. For large amount of total material these two bar like structures cannot exist instead they form one part which resembles a dog bone shaped structure.

The fillets clearly visible at the left hand side of Fig. 2(b) is also present in Fig. 2(a), however less pronounced. The fillets stems from the fact that the left hand side of the structure is clamped at the left hand side.

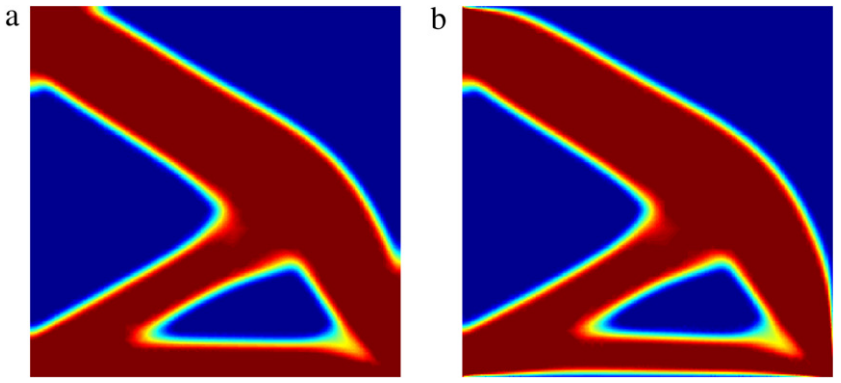

Fig. 3. The shapes of the optimal structures for material $\bar{V} = 0.5V_o$ and $\gamma_1 = 1$ and $\eta = 400$. For (a) $\gamma_2 = 0$ i.e. not penalty at design boundaries and for (b) $\gamma_2 = 200$, i.e. penalty at design boundaries. Blue color indicates void material and red full material. (For interpretation of the references to color in this figure legend, the reader is referred to the web version of this article.)

7.2. Cantilever structure

The geometry considered in the second example is shown in Fig. 1(b). The left side of the structure is clamped, i.e. homogeneous Dirichlet displacement boundary conditions is applied on the left hand side and at the lower right corner a vertical concentrated load is present. The boundary penalty term if present is applied along the top, bottom and right external boundaries. The initial material is taken a $\bar{V} = 0.5V_o$, i.e. the domain is homogeneously filled with 50% material. The material parameters are $\gamma_1 = 1$ and $\eta = 400$ and when penalty present it is set to $\gamma_2 = 200$.

From Fig. 3(a), it is concluded that for the case where no cost is present for material at design boundaries, material is preferred at the design boundaries as it tries to 'climb' upward on the lower right side. At the top left corner the same behavior can be seen as the material tries to spread out along the design boundaries.

By considering Fig. 3(b) where a cost for material on the design boundaries are present it is obvious that the attachment of material along design boundaries are not present. This is visible by comparing the right lower parts and the left top parts of the right (a) and left (b) figures. Also at the lower part of Fig. 3(b) it is shown that the material is not located along the this boundary, i.e. a completely different behavior compared to the situation when not penalty is present is obtained.

Whether there should be material located along the design boundaries is of course a question in itself. Here it is shown that if the cost for material along design boundaries is absent there are no means to control the behavior of the design. In some part it might be preferable to have material along the design boundaries, this might be the situation of the lower design boundary in Fig. 3.

Finally, the convergence history during the first 300 steps for the example illustrated in Fig. 3b is shown in Fig. 4. From Fig. 4 it can be concluded that the objective function decreases drastically during the initial phase of the optimization. This decrease stems mainly from the fact that the material reorganization results in a significantly stiffer structure. From Fig. 4 it can also be concluded that the compliance increases as the finite element discretization is refined; a result that is consistent with the fact that FE solution of the elastic problem is overestimating the stiffness of the solution, i.e. the FE method provides an upper bound solution. From Fig. 4 it can be concluded that the penalization due to F_0 is insignificant and can be omitted. It is also interesting to note that the although the absolute values the gradient energy and the boundary energy are relatively low they have a major influence on the final design.

8. Conclusions

A phase-field approach for topology optimization has been considered for the situation of maximizing the stiffness for a given amount of material. In the usual phase-field approach there is no penalty for interfaces forming at design domain boundaries and special emphasis was here devoted to associate costs to the interfaces forming at the design boundaries. Thus an augmented functional including costs for material located at the design domain boundaries has been proposed. It was shown that stationarity of the functional leads to Robin boundary condition instead of the usual Neumann boundary conditions used in a phase-field approach. In addition it was shown that adopting

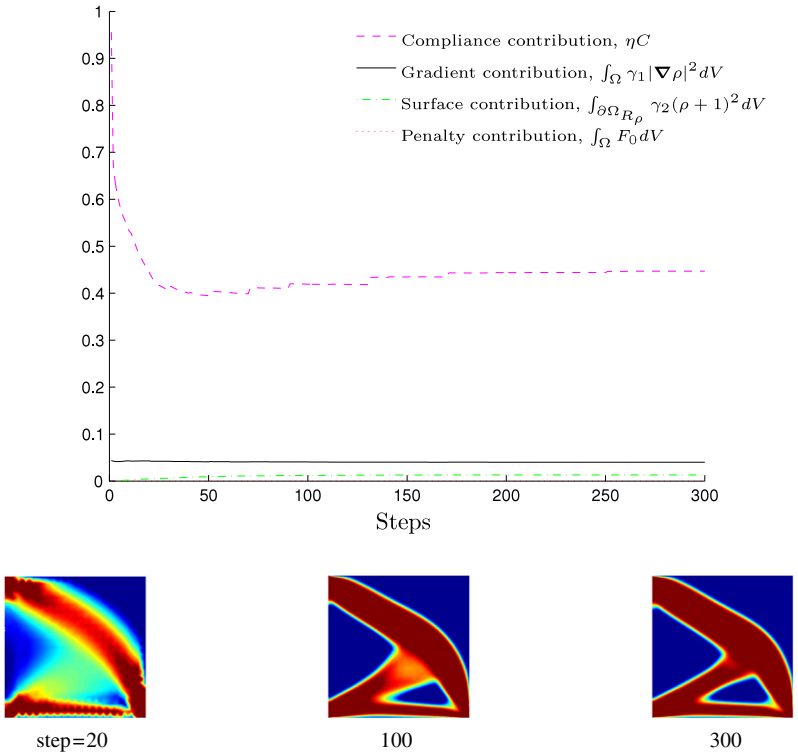

Fig. 4. Evolution of the components of the objective functional. Magenta dashed curve corresponds to the contribution due to the compliance, ηC, black solid curve corresponds to the contribution due to the gradient, $\int_\Omega \gamma_1 |\nabla \rho|^2 dV$, green dashed dotted curve corresponds to the surface contribution, $\int_{\partial\Omega_{R_\rho}} \gamma_2 (\rho+1)^2 dV$ and finally the bulk term $\int_\Omega F_0 dV$ is indicated by a dotted red curve. All contributions are normalized using the initial value of the objective functional. Snap shots of the evolution of the designs is also shown. (For interpretation of the references to color in this figure legend, the reader is referred to the web version of this article.)

a Ginzburg–Landau approach for the evolution laws together with the Robin boundary conditions minimizes the functional.

For the density field a double obstacle problem was introduced such that the density stay within the allowable range. The topology optimization problem was solved using a staggered solution strategy, where first the elastic problem was solved for constant density and then the density problem, i.e. phase-field problem was solved for constant displacements. The non-smooth problem obtained due to the double obstacle problem was then solved using a double sided version of Howard's algorithm. It was shown that the proposed solution method is well suited for solving the topology optimization problem.

Finally it was shown by solving some representative problems that the influence of costs associated with interfaces along design domains can have large impact on the solution. Two examples were considered, one which mimic uniaxial stretching and a second where a cantilever beam considered.

References

[1] M. Bendsøe, O. Sigmund, Material interpolation schemes in topology optimization, Arch. Appl. Mech. 69 (1999) 635–654.
[2] H. Eschenauen, N. Olhoff, Topology optimization of continuum structures: a review, Appl. Mech. Rev. 54 (2001) 331–390.
[3] L. Tartar, An introduction to the homogenization method in optimal design, in: Optimal Shape Design, Troia, 1998, in: Lecture Notes in Mathematics, vol. 1740, Springer-Verlag, Berlin, 2000.
[4] Y. Wang, Z. Kang, Q. He, An adaptive refinement approach for topology optimization based on separated density field description, Comput. Struct. 117 (0) (2013) 10–22.
[5] O. Sigmund, Materials with prescribed constitutive parameters: an inverse homogenization problem, Internat. J. Solids Structures 31 (17) (1994) 2313–2329.
[6] R. Haber, J. Jog, M. Bendsøe, A new approach to variable-topology shape design using a constraint on perimeter, Struct. Optim. 11 (1996) 1–12.

[7] J. Peterson, O. Sigmund, Slope constrained topology optimization, Int. J. Numer. Methods Eng. 41 (1998) 1417–1434.
[8] T. Borrvall, J. Petersson, Topology optimization using regularized intermediate density control, Comput. Methods Appl. Mech. Engrg. 190 (2001) 4911–4923.
[9] B. Bourdin, A. Chambolle, Design-dependent loads in topology optimization, ESAIM Control Optim. Calc. Var. 9 (2003) 19–48.
[10] S. Zhou, M.Y. Wang, Multimaterial structural topology optimization with generalized Cahn–Hilliard model of multiphase transitions, Struct. Multidiscip. Optim. 33 (2007) 89–111.
[11] T.E. Bruns, D.A. Tortorelli, Topology optimization of non-linear elastic structures and compliant mechanisms, Comput. Methods Appl. Mech. Engrg. 190 (2001) 3443–3459.
[12] M.Y. Wang, S. Wang, Bilateral filtering for structural topology optimization, Internat. J. Numer. Methods Engrg. 63 (13) (2005) 1911–1938.
[13] B. Bourdin, Filters in topology optimization, Internat. J. Numer. Methods Engrg. 50 (9) (2001) 2143–2158.
[14] T.E. Bruns, D.A. Tortorelli, An element removal and reintroduction strategy for the topology optimization of structures and compliant mechanisms, Internat. J. Numer. Methods Engrg. 57 (10) (2003) 1413–1430.
[15] O. Sigmund, Design of Material Structures Using Topology Optimization (Ph.D. thesis), Department of Solid Mechanics, Technical University of Denmark, Denmark, 1994.
[16] M.Y. Wang, S. Zhou, Synthesis of shape and topology of multi-material structures with a phase-field method, J. Comput.-Aided Mater. Des. 11 (2004) 117–138.
[17] J.W. Cahn, J.E. Hilliard, Free energy of a nonuniform system. I. Interfacial free energy, J. Chem. Phys. 28 (1958) 258–267.
[18] M. Wallin, M. Ristinmaa, H. Askfelt, Optimal topologies derived from a phase-field method, Struct. Multidiscip. Optim. 45 (2012) 171–183.
[19] M. Burger, R. Stainko, Phase-field relaxation of topology optimization with local stress constraints, SIAM J. Control Optim. 45 (2006) 1447–1466.
[20] L. Blank, M. Farshbaf-Shaker, H. Garcke, C. Rupprecht, V. Styles, Multi-material phase field approach to structural topology optimization, arXiv.org arXiv:1312.2356.
[21] M. Wallin, M. Ristinmaa, Howard's algorithm in a phase-field topology optimization approach, Internat. J. Numer. Methods Engrg. 94 (1) (2013) 43–59.
[22] L. Dede, M.J. Borden, T.J.R. Hughes, Isogeometric analysis for topology optimization with a phase field model, Arch. Comput. Methods Eng. 19 (2012) 427–465.
[23] L. Blank, H. Garcke, L. Sarbu, T. Srisupattarawanit, V. Styles, A. Voigt, Phase-field approaches to structural topology optimization, in: G. Leugering, S. Engell, A. Griewank, M. Hinze, R. Rannacher, V. Schulz, M. Ulbrich, S. Ulbrich (Eds.), Constrained Optimization and Optimal Control for Partial Differential Equations, in: International Series of Numerical Mathematics, vol. 160, Springer, Basel, 2012, pp. 245–256.
[24] O. Bokanowski, S. Maroso, H. Zidani, Some convergence results for Howard's algorithm, SIAM J. Numer. Anal. 47 (2009) 3001–3026.
[25] L. Blank, H. Garcke, L. Sarbu, V. Styles, Primal–dual active set methods for Allen–Cahn variational inequalities with nonlocal constraints, Numer. Methods Partial Differential Equations 29 (3) (2013) 999–1030. http://dx.doi.org/10.1002/num.21742.